AGU PUBLICATIONS

JGR

Journal of Geophysical Research: Earth Surface

RESEARCH ARTICLE
10.1002/2016JF004018

Key Points:
- GPR is competent and is a useful tool for the accurate and high-resolution detection of active layer thickness in mountainous areas
- Considerable spatial variability of active layer thickness was found owing to the variations in elevation, slope aspect, and peat layer
- Changes in active layer thickness were by greater than 80% within an area of 100 m^2 due solely to local microrelief of about 0.8 m

Correspondence to:
T. Zhang,
tjzhang@lzu.edu.cn

Citation:
Cao, B., S. Gruber, T. Zhang, L. Li, X. Peng, K. Wang, L. Zheng, W. Shao, and H. Guo (2017), Spatial variability of active layer thickness detected by ground-penetrating radar in the Qilian Mountains, Western China, *J. Geophys. Res. Earth Surf.*, *122*, 574–591, doi:10.1002/2016JF004018.

Received 5 JUL 2016
Accepted 31 JAN 2017
Accepted article online 3 FEB 2017
Published online 14 MAR 2017

Spatial variability of active layer thickness detected by ground-penetrating radar in the Qilian Mountains, Western China

Bin Cao[1,2], Stephan Gruber[2], Tingjun Zhang[1], Lili Li[1], Xiaoqing Peng[1], Kang Wang[1,3], Lei Zheng[4], Wanwan Shao[1,5], and Hong Guo[1]

[1]Key Laboratory of Western China's Environmental Systems (MOE), College of Earth and Environmental Sciences, Lanzhou University, Lanzhou, China, [2]Department of Geography and Environmental Studies, Carleton University, Ottawa, Ontario, Canada, [3]Institute of Arctic and Alpine Research, University of Colorado Boulder, Boulder, Colorado, USA, [4]Chinese Antarctic Center of Surveying and Mapping, Wuhan University, Wuhan, China, [5]Earth System Science Programme, Faculty of Science, Chinese University of Hong Kong, Hong Kong, China

Abstract The active layer plays a key role in geomorphic, hydrologic, and biogeochemical processes in permafrost regions. We conducted a systematic investigation of active layer thickness (ALT) in northeastern Qinghai-Tibetan Plateau by using ground-penetrating radar (GPR) with 100 and 200 MHz antennas. We used mechanical probing, pit, and soil temperature profiles for evaluating ALT derived from GPR. The results showed that GPR is competent for detecting ALT, and the error was ±0.08 m at common midpoint co-located sites. Considerable spatial variability of ALT owing to variation in elevation, peat thickness, and slope aspect was found. The mean ALT was 1.32 ± 0.29 m with a range from 0.81 to 2.1 m in Eboling Mountain. In Yeniu Gou, mean ALT was 2.72 ± 0.88 m and varied from 1.07 m on the north-facing slope to 4.86 m around the area near the lower boundary of permafrost. ALT in peat decreased with increasing elevation at rates of −1.31 m/km (Eboling Mountain) and −2.1 m/km (Yeniu Gou), and in mineral soil in Yeniu Gou, the rate changed to −4.18 m/km. At the same elevation, ALT on the south-facing slope was about 0.8 m thicker than that on the north-facing slopes, while the difference was only 0.18 m in peat-covered area. Within a 100 m^2 area with a local elevation difference of 0.8 m, ALT varied from 0.68 m to 1.25 m. Both field monitoring and modeling studies on spatial ALT variations require rethinking of the current strategy and comprehensive design.

1. Introduction

The active layer, defined as "the top layer of ground subject to annual thawing and freezing in areas underlain by permafrost" [*Everdingen*, 1998], plays a key role in permafrost regions as almost all biogeochemical, hydrological, ecological, geomorphic, and pedogenic processes take place in it [*Brown et al.*, 2000; *Hinzman et al.*, 1991; *Kane et al.*, 1991]. Additionally, the active layer influences ground surface energy budget and carbon exchange between the atmosphere and the land surface [*Brown et al.*, 2000; *Lemke et al.*, 2007; *Zhang et al.*, 1997]. Active layer thickness (ALT) is mainly controlled by ground surface temperature and subsurface thermal properties [*Brown et al.*, 1997; *Pang et al.*, 2009; *Zhang*, 2005]. ALT commonly ranges from less than 1 m for cold locations with insulating surface material and high subsurface ice content to near 10 m in bedrock where thermal diffusivities are high [*Farbrot et al.*, 2011; *Liu et al.*, 2012].

ALT has been systematically monitored and investigated on the Qinghai-Tibetan Plateau during the last decade [*Wu and Zhang*, 2010; *Zhao et al.*, 2010]. Mechanical probing (inserting a probe through the active layer to detect the resistance near the top of permafrost) is the most widely used method to determine the ALT in the Arctic [*Brown et al.*, 2000; *Shiklomanov et al.*, 2008; *Q. Wu et al.*, 2012]. For most locations in mountains and the Qinghai-Tibetan Plateau, however, it is unsuitable due to the prevalence of coarse soils and ALTs larger than 1.5 m. In the Qinghai-Tibetan Plateau, ALT monitoring is mainly based on the analysis of borehole temperature profiles [*Wu and Zhang*, 2008; *Zhao et al.*, 2010].

Permafrost studies in the Qilian Mountains are relatively limited and have mainly focused on thermal state and thickness [*Cheng*, 1987; *Wang et al.*, 2013; *Wang et al.*, 1995], on seasonally freeze depth [*Peng et al.*, 2016], and on permafrost carbon [*Mu et al.*, 2015; *Mu et al.*, 2014; *Mu et al.*, 2016a]. Active layer thermal regime and thickness were only investigated at a few boreholes [*Wang et al.*, 2016], and the results indicated that ALT

varied from about 1 m at Eboling sites [*Mu et al*., 2014] to about 3.7 m in Yeniu Gou [*Wang et al*., 2013]. However, its variation with soil type and topography remains largely unknown. The increasing amount of infrastructure (roads, communication, and power lines) built on permafrost adds engineering relevance to investigating ALT [*Li et al*., 2009] and makes studies of ALT of great importance. Borehole investigations are costly, in particular for a regional-scale ALT investigation, making surface measurements an important alternative. Surface measurements, on the other hand, are affected by microtopographic variation such as tussocks, frost mounds, polygons and patterned ground, or thermokarst, leading to a large variation of measured ALT over short distances [*Lemke et al*., 2007].

Geophysical methods are a suitable alternative for investigating ALT in mountains effectively and with a high number of samples. Ground-penetrating radar (GPR) is a noninvasive geophysical method suitable for permafrost studies because of the large contrast in electromagnetic properties between liquid water and ice contained in soil [*Moorman et al*., 2003]. As soil temperature decreases below 0°C, an increasing fraction of pore water exists as ice and a decreasing fraction as water. Consequently, the dielectric constant, at GPR frequencies, decreases significantly. In frozen soil, the penetration depth of electromagnetic pulses increases because energy losses due to electrical conductivity and molecular polarization decrease [*Hinkel et al*., 2001]. GPR has been widely used in polar and mountain regions for detecting shallow subsurface conditions in permafrost such as ALT [*Gusmeroli et al*., 2015; *Wu et al*., 2009], permafrost distribution [*Stevens et al*., 2009; *Wu et al*., 2005], massive ground ice [*De Pascale et al*., 2008], and pingo ice [*Yoshikawa et al*., 2006], wedge ice [*De Pascale et al*., 2008; *Hinkel et al*., 2001; *Munroe et al*., 2007], thawing depth beneath streams [*Brosten et al*., 2009; *Brosten et al*., 2006], talik zones [*Moorman et al*., 2003; *Stevens et al*., 2009], thermokarst [*De Pascale et al*., 2008], and active layer soil moisture [*Moorman et al*., 2003; *Wollschläger et al*., 2010].

The objectives of this study are (1) to apply GPR for mapping ALT in the Qilian Mountains and (2) to improve our understanding of ALT spatial variations and their environmental controls in the Qilian Mountains over northeastern Qinghai-Tibetan Plateau (Figure 1a). GPR results were evaluated by using other in situ measurements including mechanical probing, pit, and soil temperature profiles.

2. Study Area

The study area is located in the source area of Heihe River, northeastern Qinghai-Tibetan Plateau (98°31′–101°34′E and 37°45′–39°42′N°; Figure 1a). Elevations are between 1600 and 5600 m asl. Mountain ridges and valleys run from northwest to southeast (Figure 1b). The upper reaches of Heihe River Basin experienced two periods of major uplift in the Pliocene Epoch and early Quaternary, which produced the present macrogeomorphological patterns [*Li et al*., 2014]. The topography of upper reaches of Heihe River Basin is mainly controlled by faults, rift basins, and valleys that have formed between mountains [*Zhang et al*., 2014]. The sediments at the pediment plain are mainly fluvial facies.

The climate over the study area is continental and semiarid and mainly controlled by westerly winds [*Wang et al*., 2015]. Measured mean annual air temperatures in the upper reaches of Heihe River basin range from 6°C to −10°C. The annual range of air temperatures for 12 different national meteorological stations is between 26 and 39°C based on long-term mean daily observations [*Mu et al*., 2013]. Annual precipitation ranges from 250 mm to 750 mm in high mountain areas [*Zhao et al*., 2005], and the majority falls from June through September, up to 76% of annual total precipitation [*Gou et al*., 2012].

Permafrost distribution in the study area is mainly controlled by elevation [*Wang et al*., 2013] and subject to strong local modification by factors such as slope aspect, vegetation, peat layer, soil moisture and soil types, and snow cover conditions. Seasonally frozen ground in nonpermafrost areas is well developed with maximum seasonal freezing depths of greater than 2.5 m [*Peng et al*., 2016]. A permafrost observation network has been established from 2011 to 2014 in the upper reaches of the Heihe River Basin (Figure 1 and Table 1).

In Eboling Mountain, permafrost is usually found on the north-facing slopes with thick peat accumulation [*Mu et al*., 2015; *Wu et al*., 2007]. Peat layer thickness varies from 0.4 to greater than 1.0 m with average total soil organic carbon of 44 kg/m^3 and soil water content of about 60% by volume [*Mu et al*., 2015]. The lowermost observation of permafrost occurrence from a borehole in Eboling Mountain was at an elevation of around 3400 m [*Wu et al*., 2007]. According to field measurements, main vegetation types are alpine swamp meadow and alpine meadow and their distribution and conditions are significantly influenced by slope aspects and

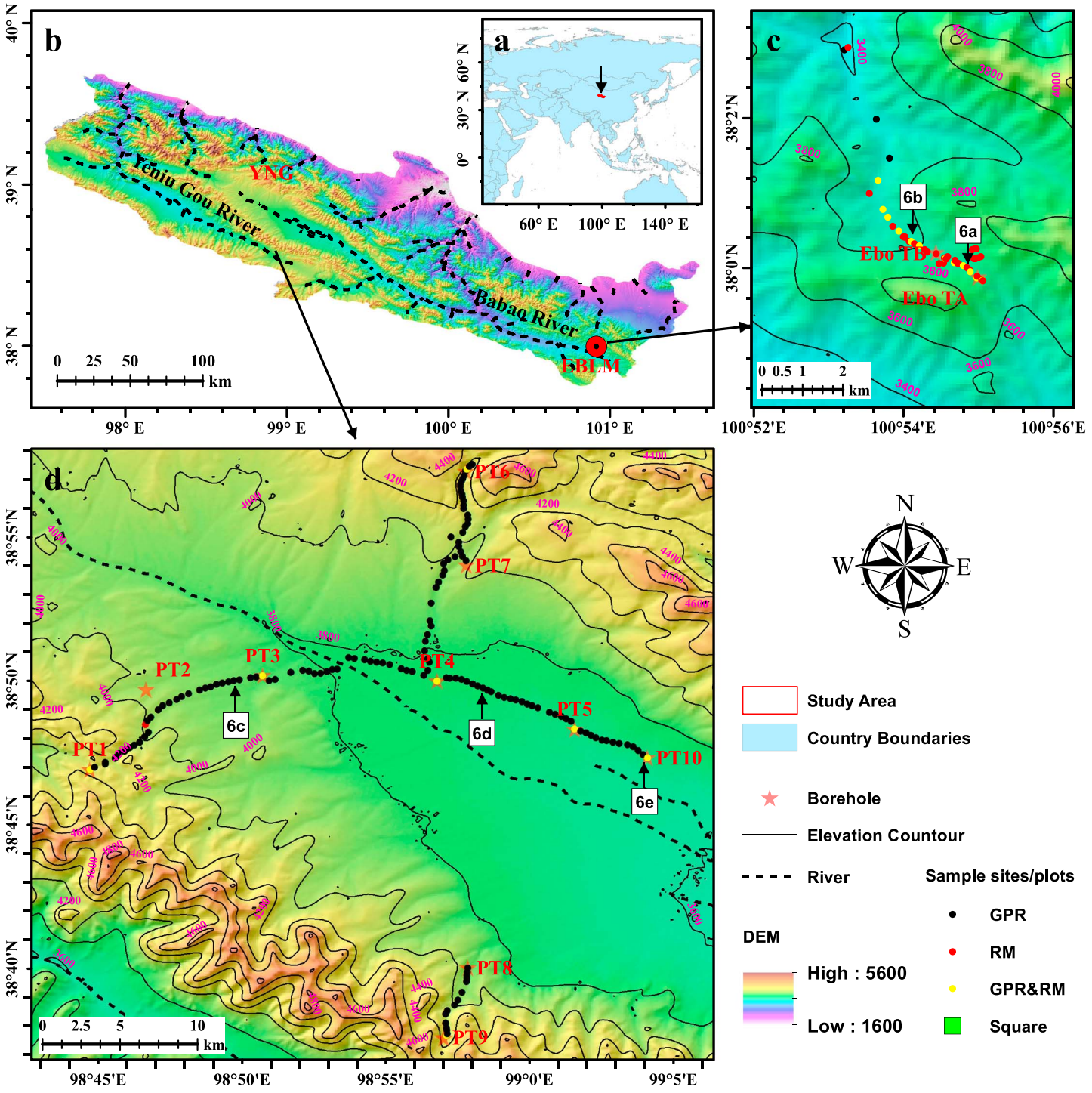

Figure 1. (a) The location of the upper reaches of Heihe River basin (study area); (b) the topography of the upper reaches of Heihe River Basin and location of Yeniu Gou and Eboling; the geographic locations of permafrost borehole sites and ALT measurement sites in (c) Eboling Mountain and (d) Yeniu Gou. RM means sites measured only by reference methods (including mechanical probing, pit, and soil temperature profiles), GPR means sample plots only measured by GPR, and GPR&RM means both of them are measured at these sites (co-located sites). The 100 m^2 quadrat location was present in Figure 1c. The selected GPR plots shown in Figure 7 are marked by an arrow in Figures 1c and 1d.

near-surface soil conditions (Figure 2). Alpine swamp meadow is usually found on the north-facing slopes with high soil moisture content and low solar radiation, while alpine meadow mainly exists on the south-facing slopes with relatively dry soils. The oval Hummocks are well developed in Eboling Mountain. In Yeniu Gou, soil is much coarser and drier with abundant gravel in areas with little or no peat content,

Table 1. Characteristics of Permafrost Borehole Sites in the Upper Reaches of the Heihe River in Western China[a]

Site	Latitude (°)	Longitude (°)	Elevation (m)	GT_{16m} (°C)	Slope Aspect	Slope Angle (°)	Observed Depth (m)	PFT (m)	Vegetation Cover	Soil Texture
PT1	98.7452	38.7822	4128	−1.88 (15 m)	NE	~6	100	~110[b]	ASM	Loam
PT2	98.7778	38.8283	3985	−0.97	NE	~6	69	62	ASM	
PT3	98.8452	38.8364	3827	−1.40	NE	Flat	50	~105[b]	AM	Loam
PT4	98.9463	38.8333	3770	−0.34	SE	Flat	90.3	23	AM	Sandy loam
PT5	99.0258	38.8054	3691	0.01	SE	Flat	20.4	13	AM	Loam
PT6	98.9627	38.9548	4153	−1.68	SE	~10	50	~175[b]	AM	Sandy clay loam
PT7	98.9630	38.9030	3970	−1.61	SW	Flat	36		ASM	Sandy loam
PT8	98.9641	38.6672	3886	−0.29	SE	~8	50	24	ASM	Loam
PT9	98.9499	38.6268	4138	−1.42 (15 m)	SE	~10	150	94	ASM	Loam
PT10	99.0679	38.7890	3681	0.06	SW	Flat	20	12	AS	Sandy loam
Ebo TA	100.9162	37.9979	3691	−0.72 (15 m)	NE	~16	20.4		ASM	Loam
Ebo TB	100.9070	38.0033	3615	−0.46 (11.5 m)	NE	~10	11.7		ASM	Loam

[a]GT_{16m}, ground temperature at 16 m depth; E, east; N, north; S, south; W, west; PFT, permafrost thickness, which was determined based on the ground temperature gradient. The permafrost thickness of PT1–PT5 is from *Wang et al*. [2013]; the information of Ebo TA and Ebo TB sites are from *Mu et al*. [2015].
[b]The borehole does not penetrate the whole permafrost layer, and the permafrost thickness was interpolated according to deep ground temperatures. ASM = alpine swamp meadow, AM = alpine meadow, AS = alpine steppe. Soil texture referred to the uppermost 0.2 m soil and was classified according to the soil taxonomy developed by the United States Department of Agriculture.

based on observations at borehole sites PT4 and PT5. There is little organic matter, and soil moisture content was about 10% or less by volume [*Wang et al*., 2013]. Permafrost occurs more widely at higher elevations with the lower boundary detected at about 3650 m [*Wang et al*., 2013; *Wu et al*., 2007]. Besides alpine swamp meadow and alpine meadow, alpine steppe is widespread in Yeniu Gou. Bare land surface and alpine desert steppe [*Chadwick and Madsen*, 2000] were also found on the south-facing slopes and near areas around the lower boundary of permafrost (Figure 3 and Table 2).

3. Data and Methods

We investigated ALT at a high number of sites to resolve the expected high spatial variation of ALT. In the sampling design, we consider main controls of ALT to be elevation, slope aspect, vegetation type, and geomorphological unit. ALT plot sites were distributed along a line between neighboring permafrost boreholes and included both the east-west (roughly parallel to mountain ridges) and north-south transects (Figures 1c and 1d). A 200 m interval between plots was used for GPR transections in sloping piedmont areas, while a 300 m interval was applied to relatively flat areas (e.g., pediment plain). Locally, this system was adjusted where necessary; for example, plots were moved to not be directly adjacent to streams and smaller intervals were used for areas where vegetation varied substantially. All plots are more than 200 m from disturbance such as roads, buildings, power lines, and communication towers. Vegetation cover was measured based on visual classification of 1 m × 1 m plot. Mean vegetation coverage ranged from more than 90% in alpine swamp meadow to less than 5% in bare land. (Figure 4)

Filed ALT measurements were conducted by using GPR, mechanical probing where possible, pit observations, and soil temperature profiles (Table 2 and Figures 2 and 5). GPR is the primary method, while data and information from the other measurements are used to evaluate GPR results. GPR profiles with unexpected attenuation were removed before further analysis. In Eboling Mountain, 11 soil pits were dug in 2011 [*Mu et al*., 2013], 3 in 2012, and 9 in 2013. All pits were dug to the depth of the permafrost table, and hence, ALTs are available. Because some data were collected in the early November when the ground was covered by snow, there is no vegetation type information for some sites. All data obtained from GPR, mechanical probing, pit, and soil temperature profiles were used to analyze ALT spatial variations and their controls over the study area.

3.1. ALT from GPR

3.1.1. Data Acquisition and Processing

Measurements were conducted with a MALÅ ProEX GPR by using 200 MHz and 100 MHz unshielded antennas from late September to November in 2014. The 200 MHz antenna was used where ALT was expected to be shallower than 2 m according to previous studies [*Andrieux et al*., 2016; *Mu et al*., 2014], while 100 MHz was

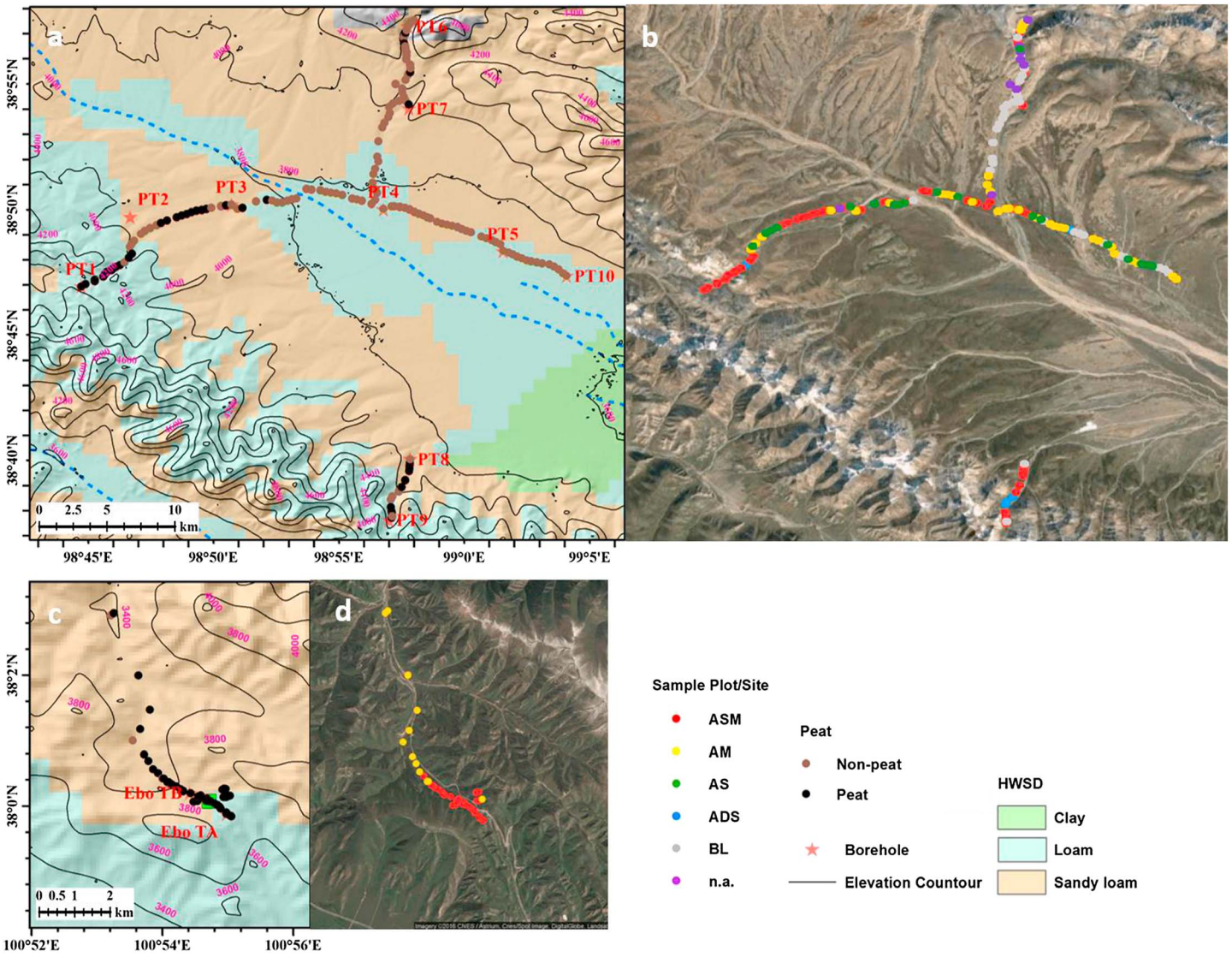

Figure 2. Peat layer information of sample plot/site shown on the background of soil texture classification from Harmonized World Soil Database (HWSD) and vegetation type on Google Earth satellite image. The spatial resolution of HWSD data sets is 30 arc sec (~1 km). (a and b) Maps of Eboling Mountain. (c and d) Maps of Yeniu Gou. ASM is alpine swamp meadow, AM is alpine meadow, AS is alpine steppe, ADS is alpine desert steppe, BL is bare land, and na means no vegetation cover information available.

used to survey larger ALT. During late September to October, the thaw depth reaches its maximum, and thus, ALT can be obtained [*Wang et al*., 2016]. In November, the near-surface soils have frozen, and at deeper layer, there is still an unfrozen layer with high amount of unfrozen water owing to the so-called "zero curtain" effect (maintaining temperatures close to the freezing point over extended periods of time in freezing or thawing soils [*Outcalt et al*., 1990]). This unfrozen layer will provide a measurable contrast to the permafrost below. The location of the plots was measured with a handheld GPS (Trimble GeoExplore 3000) with an accuracy of 1–3 m. Typically, we used common offset profiling, moving in 0.1 m intervals to collect GPR data (Figure 4a). The distances between receiver and transmitter were 0.6 m for 200 MHz and 1 m for 100 MHz. As a conversion of two-way travel time (TWTT) to depth is needed, common midpoint (CMP) surveys were collected at each plot to supplement GPR profiles. CMP analysis involves separating the transmitter and receiver by a given increment from a common midpoint [*Wollschläger et al*., 2010] (Figure 4b). During CMP surveys, a fixed moving distance from the midpoint of 0.05 m was used for both transmitter and receiver in this study. In general, each GPR section was 5 m long and the co-located CMP investigation length was

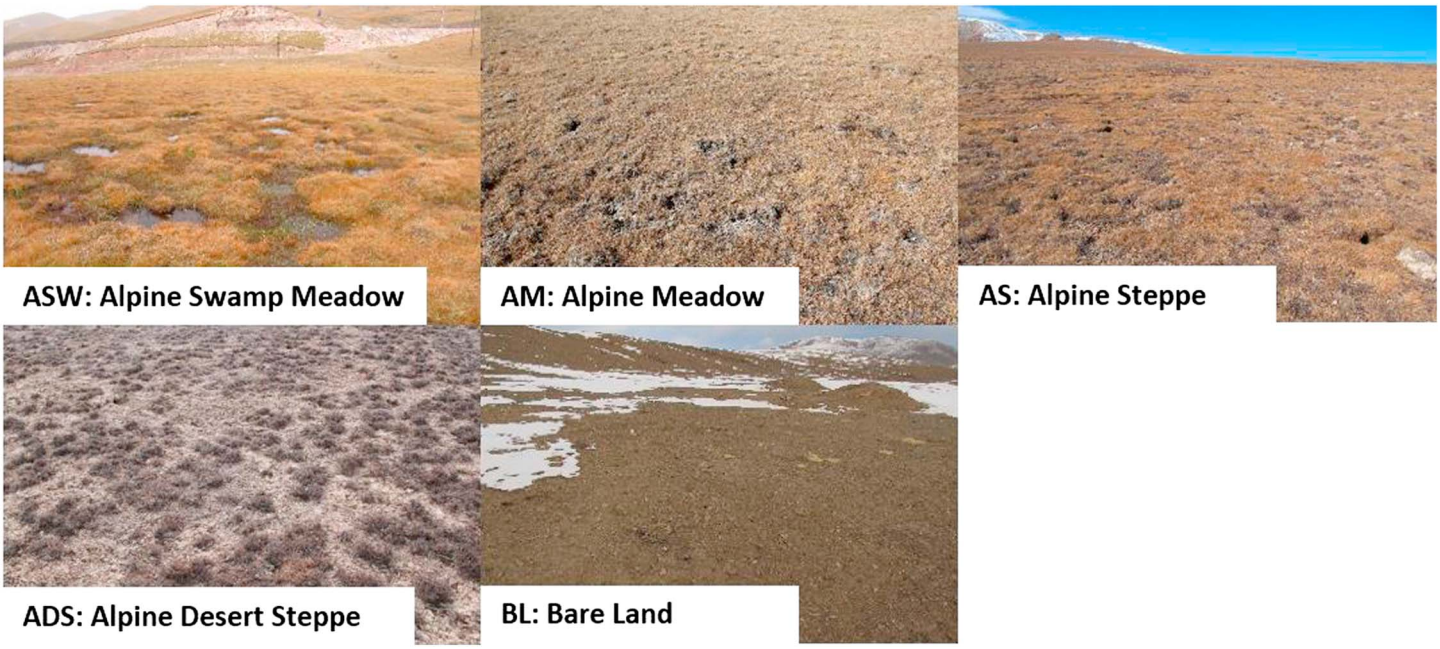

Figure 3. Field photographs showing examples of land vegetation types in the upper reaches of Heihe River Basin.

6 m. The CMP was conducted directly before or after the common offset profile measurements. We used GPR ALT data at the CMP center to represent ALT for each plot.

To investigate spatial variation at very fine scale in an area of significant surface roughness, we also obtained a dense grid of common offset observations in a 100 m^2 quadrat at Eboling Mountain (Figure 1c) during late September 2013 by using the 200 MHz antenna. This quadrat plot was measured with high density: the interval was 0.1 m in west-east direction and 0.5 m in north-south direction, resulting in 2121 GPR ALT measurements. Furthermore, microtopography was measured with a level ruler during the GPR survey, and a digital mode of the quadrat was obtained by linear interpolation.

Neal [2004] provided an in-depth discussion of GPR processing, and we applied similar procedures by using the software Reflexw (http://www.sandmeier-geo.de/reflexw.html). We used *subtract-mean* (or *dewow*) to correct signal saturation, *static correction* to adjust the time-zero position, *automatic gain control* or *energy decay* to increase the amplitudes with depth, *background removal* to remove surface-reflection, *band-pass filtering* to remove a specified frequency band (lower and upper cutoffs were set as 1/4 and 7/4 of the center frequency) from the data set, and *running average* to reduce random or high-frequency noise (Figure 4c). Not all steps were used in processing of each set of GPR measurements, as the amount of processing needed depends on raw data quality.

3.1.2. Velocity and ALT

CMP is a method for determining the mean velocity (v) in the active layer and has been successfully used in ALT investigation [*Schwamborn et al*., 2008; *T. Wu et al*., 2012]. TWTT increases with increasing separation between transmitter and receiver, resulting in a hyperbola arising from a single reflection horizon. An individual reflection of the active layer base can be picked manually from a hyperbola, and v can be obtained by using

Table 2. Summary of Field Sample Point Distribution in Eboling Mountain and Yeniu Gou

Area	No. of Sites	Elevation (m)	Method	Vegetation Type	Aspect
Eboling Mountain	48	3389–3701	GPR: 15MP[a]: 22Pit: 23	ASM: 36AM: 12	SE: 90SW: 1NE: 44NW: 15
Yeniu Gou	150	3681–4166	GPR: 150Pit: 1STP: 7	ASM: 50AM: 33AS: 19ADS: 6BL: 33na: 9	SW: 15NW: 33

[a]MP = mechanical probile, STF = soil temperature profiles, ASM = alpine swamp meadow, AM = alpine meadow, AS = alpine steppe, na = no vegetation cover information available due to the snow cover.

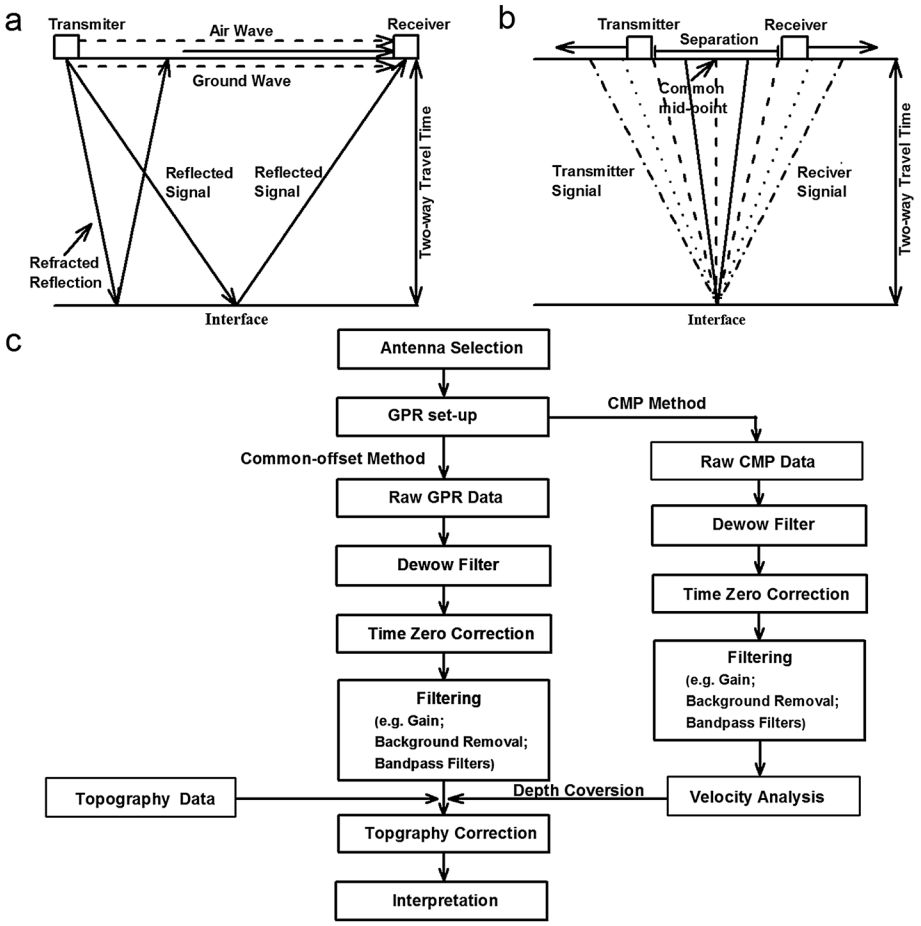

Figure 4. (a) Ray paths between transmitter and receiver for the air wave, ground wave, refracted reflection wave, and a reflected wave in the common offset profiling data acquisition mode, modified from *Fisher et al*. [1996]. (b) Common midpoint survey procedure; systematically varying antenna separation varies the signal path in the ground while keeping the point of reflection fixed, enabling wave velocity to be estimated. (c) GPR data acquisition and processing steps used in this study, modified from *Hauck and Kneisel* [2008] and *Jol* [2008]. There may be a need for adjusting some steps after processing raw GPR data to increase the visibility of the active layer base.

$$v = \sqrt{(x_2^2 - x_1^2)/(t_2^2 - t_1^2)} \tag{1}$$

where t_1 and t_2 are the TWTT of the reflection of the active layer base at the transmitter and receiver separations x_1 and x_2. Typically, x ranges from 0 to 6 m. The CMP velocity can be obtained by hyperbolic matching by using Reflexw software. ALT is then calculated from velocity and survey geometry:

$$\mathrm{ALT} = \sqrt{(vt)^2 - x^2} \tag{2}$$

where x is separation of transmitter and receiver, v is the mean velocity in the active layer, and t is TWTT of the electromagnetic wave from transmitter to receiver within the active layer. The equations used here are obtained from *Neal* [2004].

Since GPR common offset and CMP data are co-located, they can be jointly interpreted. As CMP velocities differ strongly between frozen and unfrozen sediments, the base of the active layer was easy to identify. The TWTTs in common offset profiles and CMPs are expected to be nearly identical as they use similar antenna separations.

3.2. ALT From Soil Temperature Profiles

During ALT survey, borehole temperatures were measured manually with an interval between 0.2 and 0.5 m by using a thermistor string made by the State Key Laboratory of Frozen Soil Engineering. The thermistor

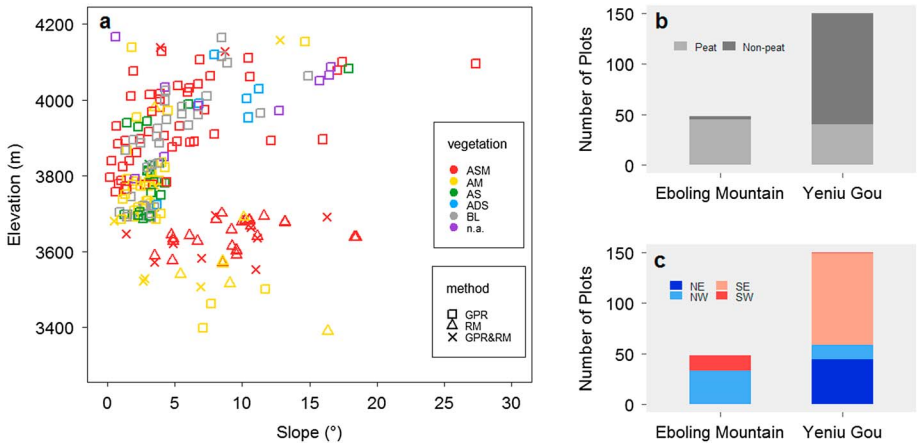

Figure 5. Overview of ALT data collected. (a) Summary of ALT plots measured by differing methods (shape) beneath diverse vegetation covers (color). (b) Number of plots measured beneath peat-covered areas and areas without peat. (c) Areas and slope exposition. RM refers to reference measurements (including STG, mechanical probing, and pit observations); GPR&RM indicates plots where GPR and reference measurements were co-located. Plots/sites in Eboling Mountains were all collected in the west-facing slope owing to the valley configuration.

string has been widely used in permafrost studies over Qinghai-Tibetan Plateau since 2003, and the temperature accuracy is ±0.05°C [*Zhao et al.*, 2010]. ALT is estimated by linear interpolation of soil temperature profiles.

3.3. ALT From Mechanical Probing and Pit Observations

Mechanical probing and pit observations were conducted in parallel with GPR measurements in peat-covered areas where ALT is small and fine soil permits probing. We also investigated the 100 m^2 quadrat by using mechanical probing at 2 m interval, resulting in 36 observations. This is because high-resolution CMP investigations in such pronounced microtopography are not operable and a reference for calculating wave propagation velocity in the quadrat was needed. Thus, ALT in the quadrat was estimated by using TWTT from GPR and velocity determined from the nearest mechanical probing point. If the GPR point is in the center of several mechanical probing sites, then the mean velocity from neighboring sites was used.

3.4. Evaluation of GPR ALT

At CMP co-located sites, the accuracy of ALT obtained from GPR was evaluated with ALT from soil temperature profiles (5 points), soil pit (1 point), and mechanical probing (13 points). In the 100 m^2 quadrat, the main uncertainty of GPR ALT likely originates from velocity variations related to soil conditions, such as moisture content, at very fine scale. The direct evaluation of this uncertainty, however, is difficult based on our data, as there is a resolution gap between GPR (0.1 m in west-east direction and 0.5 m in north-south direction) and mechanical probing (2 m) measurements. An evaluation was thus conducted at each mechanical probing location by comparing ALT determined from the velocity at this location with velocities from neighbor mechanical probing locations. This results in a measure of "potential" variation of velocity, hence ALT uncertainty within 2 m.

At co-located sites,

$$AE_{ALT} = ALT_{GPR} - ALT_{DM} \tag{3}$$

$$RE_{ALT} = \frac{ALT_{GPR} - ALT_{DM}}{ALT_{DM}} \times 100\% \tag{4}$$

where AE_{ALT} and RE_{ALT} denote the absolute and relative errors of the GPR ALT and ALT subscripts refer to direct and GPR measurements.

In the quadrat, velocity (V_{MP}) is determined at each mechanical probing site:

$$V_{MP} = 2^{*}\sqrt{ALT_{MP}{}^{2} + x^{2}}/t \quad (5)$$

where ALT_{MP} is the ALT based on mechanical probing. GPR ALTs were determined by using the velocity from nearest neighbor points and were finally evaluated based on the absolute (AE_v) and relative errors (RE_v):

$$AE_v = ALT_{GPR} - ALT_{MP} \quad (6)$$

$$RE_v = \frac{ALT_{GPR} - ALT_{MP}}{ALT_{MP}} \times 100\% \quad (7)$$

3.5. Digital Elevation Model and Geomorphological Units

The digital elevation model (DEM) used in this study has a resolution of ~90 m and was aggregated from the Global Digital Elevation Model version 2 with a grid spacing of approximately 30 m [*Tachikawa et al*., 2011]. The soil texture data set was from Harmonized World Soil Database (HWSD) with a spatial resolution of 30 arc sec (~1 km) [*Wieder et al*., 2014]. The geomorphology information used here is Geomorphological Map of China (1:4,000,000, [*Li and Li*, 1994]).

3.6. Analysis of Topoclimatic Factors

To better understand what factors control ALT and roughly predict ALT in the upper reaches of Heihe River Basin and similar mountain regions, elevation, the presence of peat, and slope aspect were selected as candidate variables for statistical testing. Unfortunately, slope aspect and consequently potential incoming solar radiation determined from the DEM were unreliable in gently sloping areas due to the fine-scale elevation noise. Thus, we simply classified slope aspect into south-facing and north-facing slopes according to point distributions (Figures 1 and 5). The influence of elevation on ALT could be simply given by

$$ALT = B_0 + \alpha_0 Ele \quad (8)$$

where ALT is given in m and Ele is elevation in m, while B_0 and α_0 are the intercept and slope of a linear model. The presence of peat significantly affects thermal conductivity of soil and hence ALT [*Fisher et al*., 2016; *Zhou et al*., 2013]. The influence of peat is incorporated in the linear model through changing slope and intercept as a function of peat coverage

$$ALT = B_0 + B_1 Peat + (\alpha_0 + \alpha_1 Peat)Ele \quad (9)$$

where Peat = 1 in peat-covered areas and Peat = 0 in area without peat; B_1 and α_1 are the peat influence on model intercept and slope. The influence of slope aspect is considered as intercept change in the model

$$ALT = B_0 + B_1 Peat + B_2 Aspect + (\alpha_0 + \alpha_1 Peat)Ele \quad (10)$$

where a north-facing slope has $B_2 = 0$ and a south-facing has $B_2 = 1$. In this case, B_2 represents the difference of ALT between south-facing and north-facing slopes. The establishment of the linear model (equation (10)) will be further discussed in section 4.3.2. The occurrence of permafrost in Eboling Mountain is significantly influenced by peat [*Mu et al*., 2016a; *Wu et al*., 2007], and almost all plots there are covered by peat (45/48; Figure 5b).

The model results were thus determined only by using data from peat-covered area, resulting only in combined values for the intercept ($B_0 + B_1$) and slope ($\alpha_0 + \alpha_1$) of the linear model. All analyses of topoclimatic factors were conducted in R (version 3.2.3).

4. Results

4.1. Evaluation of GPR ALT

The GPR ALT ranged from 1.06 to 4.86 m, and the results from reference methods were 0.8–4.84 m. At the colocated sites, the ALT range was 1.35–4.84 m or 86% of the GPR ALT range, indicating the evaluation presented here to be representative. The interpretation of common offset profiling based on CMP-derived velocity provides accurate results for investigating ALT. The absolute error is ±0.08 m when comparing GPR ALT with reference measurements (Figure 6a). The range of the relative error was from −5.3% to 3.9% with a mean of 2.7% (Figure 6c). At the quadrat in Eboling Mountain, the velocity at each mechanical probing was calculated with equation (5). The velocities at three points were low (3.34×10^{-2}, 3.55×10^{-2}, and 3.56×10^{-2} m/ns) and close to that of pure water (3.30×10^{-2} m/ns). As this is likely caused by erroneous

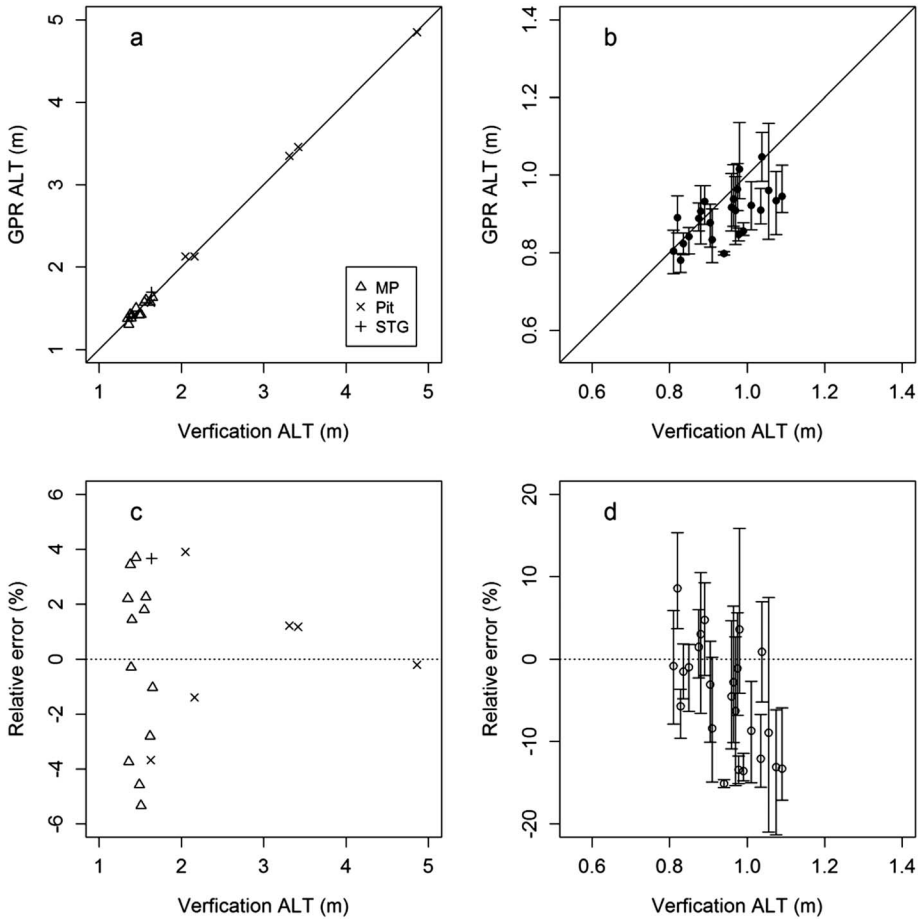

Figure 6. (a) Comparison and (c) difference between GPR interpreted based on CMP velocity and mechanical probing, pit, and soil temperature profiles for ALT. Data are on a straight line with intercept 0 and slope 1. Comparison of mechanical probing ALT and "potential" GPR ALT determined by using velocity from the nearest mechanical sites at (b) 100 m^2 quadrat and (d) the relative error. The same ALT was aggregated in Figure 6b; the point means the mean "potential" GPR ALT, while the bar refers to the range of "potential" GPR ALT at each mechanical probing site.

mechanical probing detecting shallow gravel or rock instead of the base of the active layer, we analyzed the velocity and the GPR ALT based on mechanical probing after removing these three outliers.

Figures 6b and 6d provide the potential absolute error of ALT determined by GPR in the quadrat ranged from −0.23 to 0.16 m, while the relative error ranged from −21.3% to 15.8%. For each mechanical probing site, the mean absolute error ranged from −0.15 to 0.07 m. The mean absolute error for all mechanical sites was −0.05 m, and the relative error was about −4.2%. This indicates that GPR slightly underestimates ALT in this quadrat but within confident limits. Overall, the GPR ALT in this quadrat was reliable.

4.2. GPR ALT Plots

The 200 MHz measurements recovered ALT down to 2 m in peat layer with a strong and continuous reflection (Figures 7a and 7b). The 100 MHz measurements achieved good success for ALT between 2 and 5 m with soil types of loam and gravel. Reflections at Yeniu Gou were more complex due to stronger variation of soil characteristics. In general, the interface between frozen and unfrozen soils showed a strong horizontal reflection, making the active layer base easy to identify. Sometimes the reflection was degraded by noise from point (e.g., gravel) and horizontal (e.g., variation of sediment texture) reflections and became unclear. For example, ALT shows a clear reflection for 0–0.8 m and 1–3.2 m in Figure 7c but is hard to discern in the other parts. This discontinuous reflection is also visible in Figure 7d (2–2.4 and 3–3.2 m) and Figure 7e (3.8–4.2 m). CMP proved suitable for determining velocities and for jointly interpolation (Figure 8). For example, the TWTT of active layer base with an antenna separation of 0.6 m in Figure 8a is close to the TWTT at 2.5 m (CMP

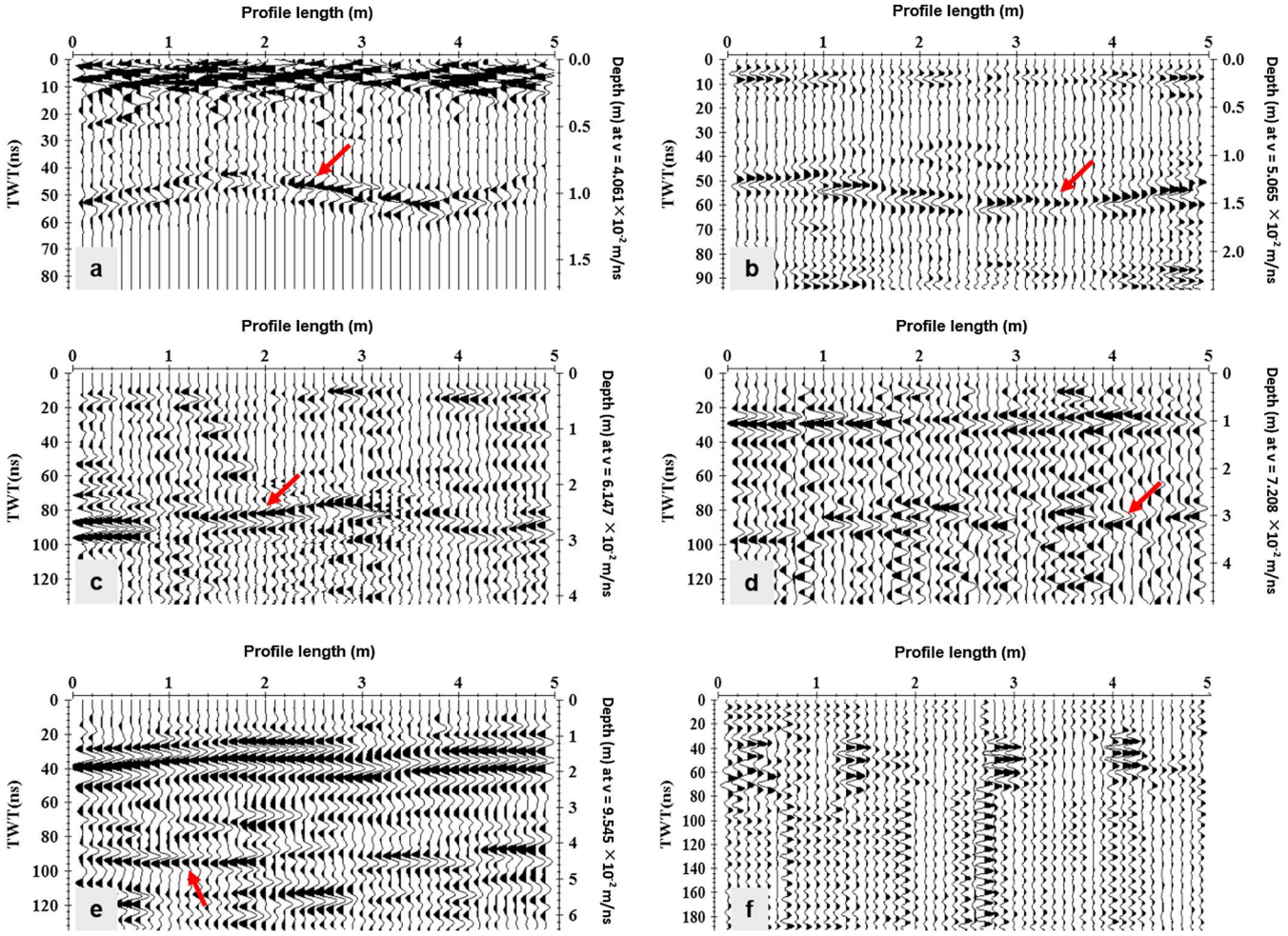

Figure 7. Processed radargram of differing GPR sections. The reflection of the active layer is marked by an arrow. The sections show reflections at the active layer base, but there is no visible reflection at the last location. The locations have ALTs of (a) 0–1 m, (b) 1–2 m, (c) 2–3 m, (d) 3–4 m, and (e) 4–5 m. (f) Collected at 200 MHz; the others are collected at 100 MHz. Figures 7a and 7b are from Eboling Mountain (peat-covered), while the other radargrams were collected in Yeniu Gou (nonpeat). The locations of Figures 7a–7e plots could be found in Figure 1. Figure 7f was removed before further analysis and was not present in Figure 1. By getting away from the middle of the profile (CMP measurement point), the accuracy of ALT is expected to decrease because of the potential uncertainty of velocity caused by changes of soil conditions. In order of the figures the clarity of the reflection hence, ALT, decreases since the reflections are interpreted as frost tables going weaker.

investigation point) in Figure 7b. This provides an additional indication for the robustness of this GPR interpretation.

4.3. Spatial Variations of ALT

4.3.1. In-Suit Measured ALT

In our study area, the main factors controlling ALT are elevation, slope aspects, soil types, peat layer, and vegetation (Figure 9). ALT decreases with elevation at a rate of about -5 ± 0.3 m/km in Yeniu Gou and about -1.9 ± 0.5 m/km in Eboling Mountain. The different rates of ALT changes with elevation are strongly controlled by other factors such as the presence of peat and vegetation. The effect of vegetation on ALT is complicated, but in general, areas with dense vegetation have shallower ALT than those with sparse or no vegetation. However, exceptions to this were noted in the study area. For example, there is no clearly change of ALT around site PT2 where vegetation changes from alpine swamp meadow to alpine meadow and to alpine steppe. The presence of a peat layer clearly is a major factor to reduce ALT in the study area.

The combined analysis of controlling factors provides a clearer picture on the spatial variation of ALT in the upper reaches of Heihe River Basin in northeastern Qinghai-Tibetan Plateau. Vegetation cover, soil texture, and the presence of a peat layer are largely influenced by slope aspect (Table 1 and Figure 2). Thus,

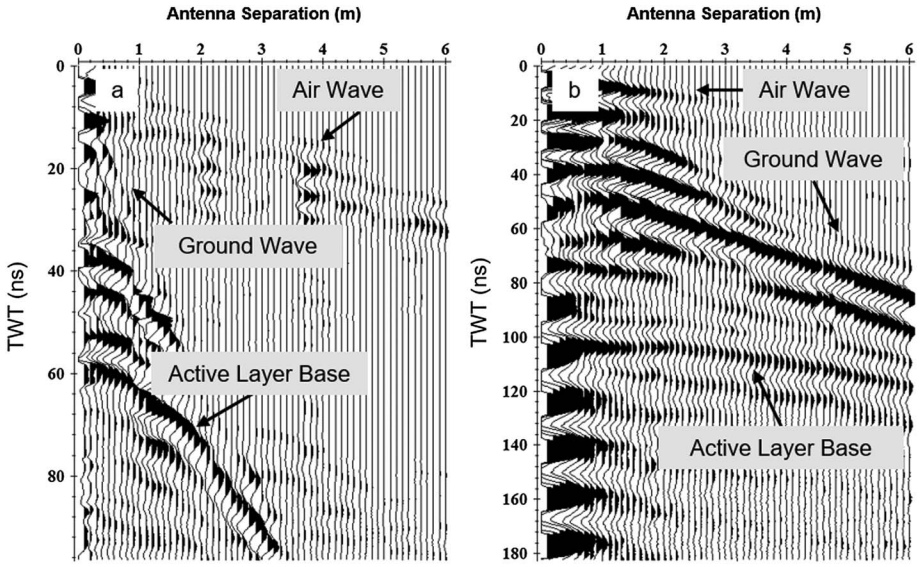

Figure 8. CMP profile with air wave, ground wave, and reflection from the active layer base. (a) Co-located with the one shown in Figure 7b. (b) Co-located with the one shown in Figure 7e.

shallower ALT was found on the north-facing slopes (e.g., from PT1 to PT2 and in Eboling Mountain) with fine soil (loam), dense vegetation, and the presence of a peat layer, while a larger ALT was found on the south-facing slopes (e.g., from PT6 to PT4) and valleys (e.g., from PT4 to PT10) with coarser soil (sandy loam/sandy clay loam), sparse vegetation, and without a peat layer. A clearly increase of ALT was found around PT3 site due mainly to the changes of the slope aspect.

In Yeniu Gou, ALT ranged from 1.07 m on the north-facing slopes to 4.86 m near the area around the lower boundary of permafrost with a mean ALT of 2.72 ± 0.88 m (Figure 9a). The mean ALTs are about 2.14 ± 0.61 m for alpine swamp meadow, about 3.13 ± 0.79 m for alpine meadow, about 3.09 ± 1.02 m for alpine steppe, about 2.29 ± 0.81 m for alpine desert steppe, and about 3.16 ± 0.81 m for bare land.

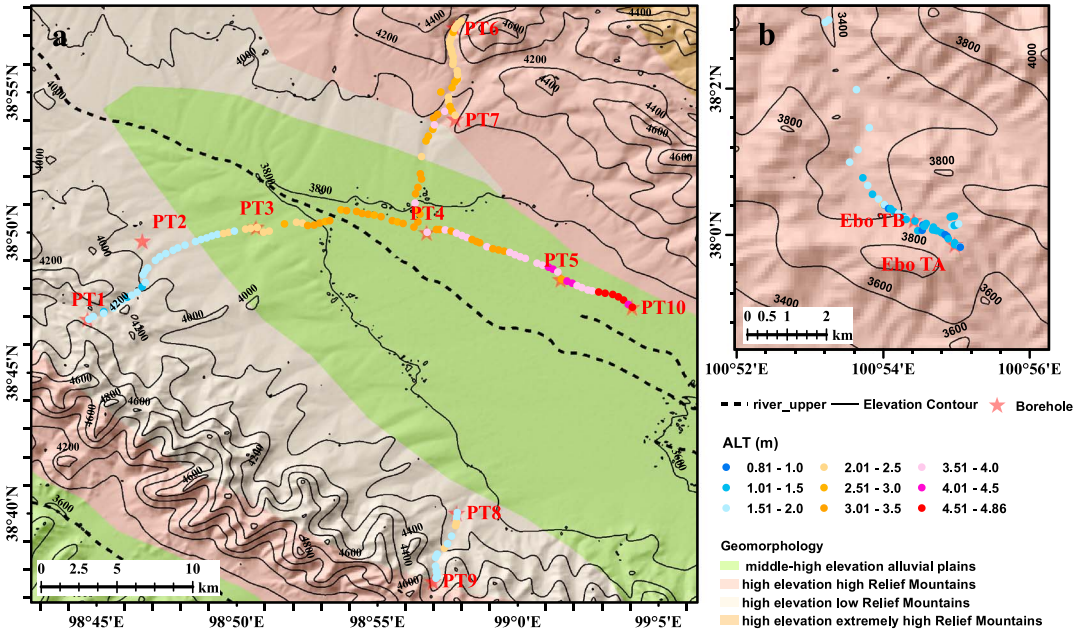

Figure 9. Spatial variation of measured ALT in (a) Yeniu Gou and (b) Eboling Mountain shown on the background of geomorphology at a scale of 1:4,000,000.

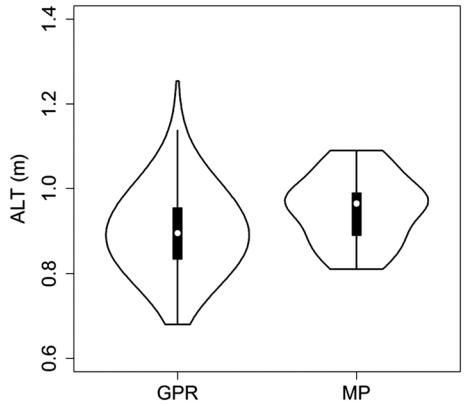

Figure 10. ALT range determined from GPR and mechanical probing in the 100 m^2 quadrat.

In Eboling Mountain, the observed ALT varied between 0.81 m and 2.1 m with the mean value of 1.32 ± 0.29 m and was predominately less than 2 m at the collected points during 2011–2014 (Figure 9b). The mean ALT was 1.22 ± 0.24 m in alpine swamp meadow and was 1.63 ± 0.22 m in alpine meadow. The mean ALT in Yeniu Gou is about twice of that in Eboling Mountain, even though average elevation in Yeniu Gou is much higher than that of Eboling Mountain. The shallower ALT in Eboling Mountain is mainly because of the presence of thick peat and the predominance of the north-facing slopes in the sample set.

In the 100 m^2 quadrat, the mean ALT was 0.9 ± 0.07 m based on GPR and about 0.95 ± 0.08 m based on mechanical probing. This difference is within 6%. The high-resolution GPR measurements showed a wider ALT range (0.68 to 1.25 m than the mechanical probing and 0.81 to 1.09 m; Figure 10). GPR ALT is mainly in the range from 0.7 to 1.1 m, occupying about 97.8% of the area. This implies that GPR method can resolve the spatial variation of ALT at a finer scale. Local surface roughness and elevation varied by 0.8 m within the 100 m^2 according to topography data (Figure 11a), while GPR ALT in such a small area varied by a difference of greater than 80% (Figure 11b).

4.3.2. Statistical Linear Model

The results of fitting a linear model (Figure 12) quantify the ALT decrease with the elevation. In addition, peat could significantly affect the slope and intercept of the linear model, while only the intercept was clearly different on the south-facing and north-facing slopes. Thus, the linear model was established as equation (10). As a result, the model results are significant ($p < 0.05$) (Table 3).

In Yeniu Gou, the linear model indicated combination of topoclimatic factors (elevation, slope aspect, and the presence of peat), explaining 84% (adjusted $R^2 = 0.84$) of the variation in ALT. Model coefficients for Yeniu Gou indicate that a difference in elevation of 100 m is equivalent to a change of 0.42 m in ALT in areas without

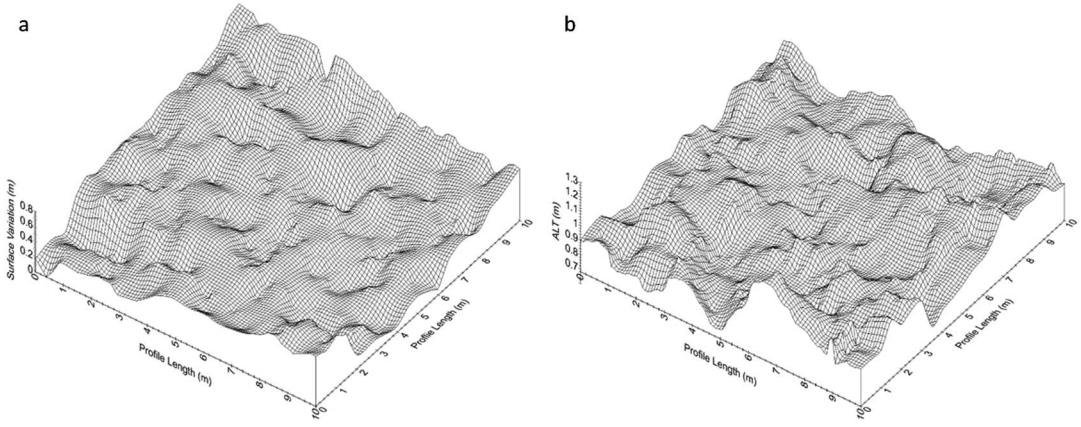

Figure 11. 3-D variation of (a) surface and (b) GPR ALT at the 100 m^2 quadrat. ALT was calculated by using TWTT from GPR and velocity determined from the nearest mechanical probing points.

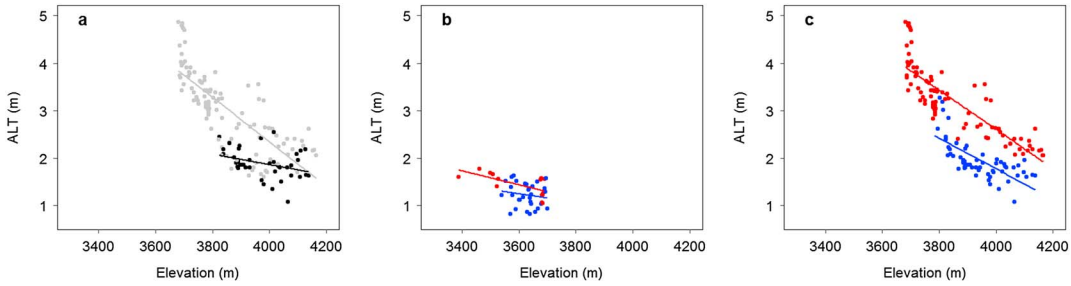

Figure 12. ALT as a function of elevation plotted with best fit lines. (a) The influence of peat on ALT in Yeniu Gou. The black point represents peat-covered plots, while the gray point represents plots without peat. The influence of aspect on ALT in (b) Eboling Mountain and in (c) Yeniu Gou. The north-facing slopes are shown in blue, while the south-facing slopes are shown in red.

peat and to only half of that (or about 0.21 m) where peat is present. ALT beneath south-facing slopes was on average about 0.8 m larger than beneath the north-facing slopes. This is equivalent to a decrease of elevation by 190 m (380 m) in areas without peat (with peat).

In Eboling Mountain, elevation and slope aspects explained 23% (adjusted $R^2 = 0.23$) of the spatial variation of ALT. The lower R^2 in Eboling Mountain than in Yeniu Gou is likely caused by a smaller range in measured elevation, whereby observed differences potentially relate more to unmeasured variables such as soil moisture and snow cover. Further field measurements are needed for better comprehension. Model coefficients at Eboling Mountain indicate that a change in elevation of 100 m in peat-covered areas is equivalent to a difference in ALT of 0.13 m. ALT is on average 0.18 m larger on south-facing than on the north-facing slopes. This implies that the change of slope aspects is equivalent to a difference of 138 m in elevation.

5. Discussion

5.1. Advantages and Disadvantages of GPR

Economic development in this part of Asia is growing, and detailed knowledge about permafrost distribution and ALT is important from engineering and environmental points of view (e.g., in order to limit thermokarst) [*Lin et al*., 2010; *Niu et al*., 2011]. However, investigation of ALT is usually limited to interpreting borehole temperature profiles as coarse-grained soil and large ALT often preclude manual probing. As boreholes are costly, only few ALT observations are usually available even though the spatial variations of ALT in mountain regions are known to be large, owing to varying topography, vegetation cover, and soil conditions. This is important because ALT changes measured by sparsely distributed boreholes in a large area would likely underestimate the true variability that is better revealed by observations at finer scale in much smaller area. For example, the ALT difference was ~2.1 m along the Qinghai-Tibetan Highway (more than 600 km long in permafrost regions) based on measurements from 30 borehole monitoring sites [*Zhao et al*., 2010], which is much smaller than the difference of ~4 m in the upper reaches of Heihe River Basin (within a 35 km radius).

This study shows that GPR could reveal the high-resolution spatial variation of ALT at a regional scale (e.g., ~35 km × 35 km in Yeniu Gou) in mountains with acceptable error (within ±0.08 m or ±5.3%; Figure 9). GPR

Table 3. Model Parameters and Correlation Matrix Between Influence Factors and ALT[a]

Topoclimatic Factor	Model Parameter	Eboling Mountain	Yeniu Gou
Elevation slope [m/km]	α_0	−1.31**(combined)	−4.18**
Elevation slope: peat [m/km]	α_1		−2.10**
Intercept	B_0	5.97*(combined)	18.51**
Peat intercept	B_1		−8.44**
South-facing slope	B_2	0.18*	0.80**

[a]Combined value in Eboling Mountain refers to the sum value of the slope and intercept in the model. The units for the topoclimatic variables are given in square brackets for each coefficient.
*$p < 0.05$.
**$p < 0.01$

is an inexpensive and fairly accurate way to characterize ALT in coarse-grained soil, either as point, transects, or as a grid of measurements. It should be considered as an important tool prior to development in similar mountain ranges. This can make the ALT observations in mountain regions more comparable to Arctic sites where ALT is usually estimated from grid measurements as used in the Circumpolar Active Layer Monitoring program [*Andrieux et al*., 2016]. In peat-covered areas, direct measurements are easily applicable; however, GPR can better resolve ALT variations at a finer scale.

Our high-resolution ALT measurements showed strong ALT variations in small areas such as the 100 m^2 quadrat. The results have a degree of uncertainty introduced by the small number of velocity measurements compared to the number of GPR observations. Variation of soil characteristics, e.g., soil moisture, would directly imply variations in dielectric constant, hence, velocity, resulting in uncertainty of ALT. Soil moisture content is expected to be a key factor controlling ALT. Its importance stems from its influence on latent heat of fusion as well as on soil thermal conductivity. GPR-based soil moisture measurement has been successfully applied in different types of soil in both the Arctic [*Gacitua et al*., 2010; *Parsekian et al*., 2012] and mountain regions [*Ma et al*., 2012; *Wollschläger et al*., 2010]. Multichannel GPR can provide continuous profiles of velocity and TWTT and hence estimates of both ALT and soil moisture [*Westermann et al*., 2010; *Wollschläger et al*., 2010]. This is important for distinguishing the mechanisms by which climate and surface changes affect ALT. Both soil moisture and ALT can react to changes in air temperature and precipitation or in plant cover as this affects evaporation and shading. GPR is well suited to detect ALT; it fails at some sites due to unexpected attenuation (Figure 7f). GPR measurements are limited by soil conditions such as high salinity or high clay content. As the strength of GPR in periglacial environments derives from the dielectric contrast between liquid water and ice, it may be challenging to obtain ALT in places where soil content is very low. In addition, strong variation in topography and ALT will increase errors due to lateral reflections [*Neal*, 2004].

Finally, the interpretation of ALT measurements as an indication of climate change effects may be misleading when there is ground subsidence due to the melt of excess ice [*Liu et al*., 2012; *Liu et al*., 2010]. This is important as thermokarst (2 m deep and ~2–3 km length) has been observed in Eboling Mountain [*Mu et al*., 2016b]. As such, it would be good to use accurate differential global positioning system and benchmarks for annual repeat surveys, so that both changes in ALT and changes in surface elevation can be recorded.

5.2. Uncertainty of Linear Model

Even using the most basic method (e.g., Stefan solution and the temperature at the top of permafrost model), estimating ALT requires good knowledge of climate (e.g., air temperature) and soil conditions (e.g., thermal conductivity and soil moisture content) [*Smith and Riseborough*, 2002; *Zhang et al*., 2005], which are usually not available or largely unknown in mountain regions. In this study, we used a simple linear model to calculate ALT, which considers elevation, peat, and slope aspect (Table 3). These three topoclimatic factors are selected here to partly respond to the variations of air temperature and soil condition in mountain regions. The model is useful in the Heihe River Basin and similar mountain regions as the required input parameters could be easily measured in the field, and hence, ALT could be roughly obtained. In addition, spatial interpolation of ALT pattern could be obtained once the areas of peat cover are detected and described.

Although the model was carefully established by a high number of filed measurements and our results showed significant relationships between ALT and topoclimatic factors (Table 3 and Figure 12), the validity of the linear relationship outside the study area and the surface types observed is still under debate and cannot be evaluated from this study. The linear model was established heavily based on statistical results, and hence, the accuracy is influenced by distribution of sample sites (e.g., the R^2 in Eboling Mountain is 0.23, owing to the low range of sample sites in elevation). Moreover, ALT is site specific and usually depends not only on elevation, peat cover, and slope aspect but also on many additional variables like soil moisture content, snow cover, and vegetation cover. To improve the understanding of ALT spatial pattern, more in-depth knowledge of climate and soil conditions at both site-specific and spatial scales should be considered in the future.

6. Conclusions

Systematic investigation of ALT was carried out in the upper reaches of Heihe River Basin during 2013 and 2014 by using GPR, direct measurements (mechanical probing and pit), and soil temperature profiles. Our results support seven conclusions:

1. Observed ALT in the upper reaches of Heihe River Basin varied from less than a meter to nearly 5 m. The mean ALT in Eboling Mountain was about 1.32 ± 0.29 m with a range from 0.81 to 2.1 m. The mean ALT in Yeniu Gou was about 2.72 ± 0.88 m with a range from 1.07 to 4.86 m. The mean ALT in Eboling Mountain is only about half of ALT in Yeniu Gou due mainly to the presence of thick peat layer and the effect of the north-facing slope.
2. Over a 100 m^2 quadrat with a local elevation difference of about 0.8 m and all other conditions are relatively homogenous; the ALT varied from 0.68 to 1.25 m, a huge difference greater than 80%, indicating that spatial variations of ALT are much more complicated. Both field monitoring and modeling studies on spatial ALT variations will require rethinking of the current strategy and comprehensive design.
3. Observed ALT is mainly controlled by elevation and the presence of peat layer over the study area. Overall, ALT increased with decreasing elevation. ALT elevation gradient for Eboling Mountain was about −1.31 m/km and for Yeniu Gou area about −2.1 m/km in peat-covered areas, while ALT variation was about −4.18 m/km with no peat layer in Yeniu Gou.
4. ALT was significantly thinner on the north-facing slopes than on the south-facing slopes. Without peat layer, ALT is about 0.8 m thicker on the south-facing slopes than on the north-facing slopes, while with a peat layer, the difference is reduced to about 0.18 m.
5. ALT changes substantially with different vegetation types. The mean ALT was about 2.14 ± 0.61 m for alpine swamp meadow, about 3.13 ± 0.79 m for alpine meadow, about 3.09 ± 1.02 m for alpine steppe, about 2.29 ± 0.81 m for alpine desert steppe, and about 3.17 ± 0.81 m for bare land in Yeniu Gou, while the mean ALT was about 1.22 ± 0.24 m for alpine swamp meadow and about 1.63 ± 0.22 m for alpine meadow in Eboling Mountain.
6. Overall, thinner active layer was found on the north-facing slopes with fine soils and higher soil moisture content, dense vegetation, and the presence of peat layer, while relatively thicker ALT was found on the south-facing slopes and valleys with coarser drier soils, sparse vegetation, and the absence of peat layer.
7. GPR is an inexpensive way to characterize ALT over mountain regions with good confidence, where direct methods (e.g., mechanical probing and borehole investigation) are difficult to apply or expensive. The absolute error of GPR ALT was ±0.08 m with relative errors ranging from −3.9 to 5.3%. The mean relative error was about 2.7% in the 100 m^2 quadrat.

Acknowledgments

We would like to express our gratitude to the colleagues for their help with fieldwork and Alessio Gusmeroli from the University of Alaska Fairbanks for his helpful advice in GPR choice. Thanks for the valuable and constructive comments and suggestions from Gregory De Pascale and the anonymous reviewer. This study was supported by the National Natural Science Foundation of China (91325202), the National Key Scientific Research Program of China (2013CBA01802), and partly by the Fundamental Research Funds for the Central Universities. The Harmonized World Soil Database data set and Geomorphological Map of China data set are provided by the Environmental and Ecological Science Data Center for West China and the National Natural Science Foundation of China (http://westdc.westgis.ac.cn). All data and information applied in this paper are available from the authors upon request (caob08@lzu.edu.cn).

References

Andrieux, E., P. Bertran, and K. Saito (2016), Spatial analysis of the French Pleistocene permafrost by a GIS database, *Permafrost Periglacial Processes*, *27*(1), 17–30, doi:10.1002/ppp.1856.

Brosten, T. R., J. H. Bradford, J. P. McNamara, J. P. Zarnetske, M. N. Gooseff, and W. B. Bowden (2006), Profiles of temporal thaw depths beneath two arctic stream types using ground-penetrating radar, *Permafrost Periglacial Processes*, *17*(4), 341–355.

Brosten, T. R., J. H. Bradford, J. P. McNamara, M. N. Gooseff, J. P. Zarnetske, W. B. Bowden, and M. E. Johnston (2009), Estimating 3-D variation in active-layer thickness beneath arctic streams using ground-penetrating radar, *J. Hydrol.*, *373*(3), 479–486.

Brown, J., O. J. Ferrians, J. Heginbottom, and E. Melnikov (1997), *Circum-Arctic map of permafrost and ground-ice conditions*, U.S. Geol. Surv., Reston, Va.

Brown, J., K. M. Hinkel, and F. Nelson (2000), The circumpolar active layer monitoring (calm) program: Research designs and initial results1, *Polar Geogr.*, *24*(3), 166–258, doi:10.1080/10889370009377698.

Chadwick, W. J., and J. A. Madsen (2000), The application of ground-penetrating radar to a coastal prehistoric archaeological site, Cape Henlopen, Delaware, USA, *Geoarchaeology*, *15*(8), 765–781, doi:10.1002/1520-6548(200012)15:8<765::AID-GEA2>3.0.CO;2-H.

Cheng, G. (1987), The distribution of permafrost in the Qilian Mountains, in *Reports in the Northeastern Part of the Qinghai-Xizang (Tibet) Plateau*, pp. 316–342, Science Press, Beijing.

De Pascale, G. P., W. H. Pollard, and K. K. Williams (2008), Geophysical mapping of ground ice using a combination of capacitive coupled resistivity and ground-penetrating radar, Northwest Territories, Canada, *J. Geophys. Res.*, *113*, F02S90, doi:10.1029/2006JF000585.

Everdingen, R. O. V. (1998), Multi-language glossary of permafrost and related ground-ice terms in Chinese, English, French, German, Icelandic, Italian, Norwegian, Polish, Romanian, Russian, Spanish, and Swedish International Permafrost Association, Terminology Working Group.

Farbrot, H., T. F. Hipp, B. Etzelmüller, K. Isaksen, R. S. Ødegård, T. V. Schuler, and O. Humlum (2011), Air and ground temperature variations observed along elevation and continentality gradients in southern Norway, *Permafrost Periglacial Processes*, *22*(4), 343–360, doi:10.1002/ppp.733.

Fisher, J. P., C. Estop-Aragones, A. Thierry, D. J. Charman, S. A. Wolfe, I. P. Hartley, J. B. Murton, M. Williams, and G. K. Phoenix (2016), The influence of vegetation and soil characteristics on active-layer thickness of permafrost soils in boreal forest, *Global Change Biol.*, doi:10.1111/gcb.13248.

Fisher, S. C., R. R. Stewart, and H. M. Jol (1996), Ground penetrating radar (GPR) data enhancement using seismic techniques, *J. Environ. Eng. Geophys.*, *1*(2), 89–96.

Gacitua, G., M. P. Tamstorf, and S. Lee (2010), Using ground penetrating radar to estimate active layer moisture conditions in the Arctic paper presented at Ground Penetrating Radar (GPR), 2010 13th International Conference on, IEEE.

Gou, X., F. Zhang, Y. Deng, G. J. Ettl, M. Yang, L. Gao, and K. Fang (2012), Patterns and dynamics of tree-line response to climate change in the eastern Qilian Mountains, northwestern China, *Dendrochronologia*, *30*(2), 121–126, doi:10.1016/j.dendro.2011.05.002.

Gusmeroli, A., L. Lin, K. Schaefer, T. Zhang, T. Schaefer, and G. Grosse (2015), Active layer stratigraphy and organic layer thickness at a thermokarst site in Arctic Alaska identified using ground penetrating radar, *Arct. Antarct. Alp. Res.*, *47*(2), 195–202.
Hauck, C., and C. Kneisel (2008), *Applied Geophysics in Periglacial Environments*, Cambridge Univ. Press, Cambridge.
Hinkel, K., J. Doolittle, J. Bockheim, F. Nelson, R. Paetzold, J. Kimble, and R. Travis (2001), Detection of subsurface permafrost features with ground-penetrating radar, Barrow, Alaska, *Permafrost Periglacial Processes*, *12*(2), 179–190.
Hinzman, L., D. Kane, R. Gieck, and K. Everett (1991), Hydrologic and thermal properties of the active layer in the Alaskan Arctic, *Cold Reg. Sci. Technol.*, *19*(2), 95–110.
Jol, H. M. (2008), Ground penetrating radar theory and applications Access Online via Elsevier.
Kane, D. L., L. D. Hinzman, and J. P. Zarling (1991), Thermal response of the active layer to climatic warming in a permafrost environment, *Cold Reg. Sci. Technol.*, *19*(2), 111–122.
Lemke, P., J. Ren, R. B. Alley, I. Allison, J. Carrasco, G. Flato, Y. Fujii, G. Kaser, P. Mote, and R. H. Thomas (2007), Observations: Changes in snow, ice and frozen ground, in *Climate Change 2007: The Physical Science Basis; Summary for Policymakers, Technical Summary and Frequently Asked Questions. Part of the Working Group I Contribution to the Fourth Assessment Report of the Intergovernmental Panel on Climate Change*, pp. 337–383, Cambridge Univ. Press, Cambridge, U. K., and New York.
Li, B., and J. Li (1994), *1:4,000,000 Geomorphological Map of China*, Science Press, Beijing.
Li, J., Y. Sheng, J. Wu, J. Chen, and X. Zhang (2009), Probability distribution of permafrost along a transportation corridor in the northeastern Qinghai province of China, *Cold Reg. Sci. Technol.*, *59*(1), 12–18, doi:10.1016/j.coldregions.2009.05.012.
Li, J., Y. Sheng, J. Chen, J. Wu, and S. Wang (2014), Variations in permafrost temperature and stability of alpine meadows in the source area of the Datong River, northeastern Qinghai-Tibet Plateau, China, *Permafrost Periglacial Processes*, *25*(4), 307–319, doi:10.1002/ppp.1822.
Lin, Z., F. Niu, Z. Xu, J. Xu, and P. Wang (2010), Thermal regime of a thermokarst lake and its influence on permafrost, Beiluhe Basin, Qinghai-Tibet Plateau, *Permafrost Periglacial Processes*, *21*(4), 315–324.
Liu, L., T. Zhang, and J. Wahr (2010), InSAR measurements of surface deformation over permafrost on the North Slope of Alaska, *J. Geophys. Res.*, *115*, F03023, doi:10.1029/2009JF001547.
Liu, L., K. Schaefer, T. Zhang, and J. Wahr (2012), Estimating 1992–2000 average active layer thickness on the Alaskan North Slope from remotely sensed surface subsidence, *J. Geophys. Res.*, *117*, F01005, doi:10.1029/2011JF002041.
Ma, Y., Y. Zhang, S. B. Farhan, and Y. Guo (2012), Permafrost soil water content evaluation using high-frequency ground-penetrating radar in Amdo catchment, Central Tibetan Plateau paper presented at Ground Penetrating Radar (GPR), 2012 14th International Conference on, 4–8 June 2012.
Moorman, B. J., S. D. Robinson, and M. M. Burgess (2003), Imaging periglacial conditions with ground-penetrating radar, *Permafrost Periglacial Processes*, *14*(4), 319–329.
Mu, C., T. Zhang, B. Cao, X. Wan, X. Peng, and G. Cheng (2013), Study of the organic carbon storage in the active layer of the permafrost over the Eboling Mountain in the upper reaches of the Heihe River in the Eastern Qilian Mountains, *J. Glaciol. Geocryol.*, *35*(1), 1–9.
Mu, C., T. Zhang, Q. Wu, X. Zhang, B. Cao, Q. Wang, X. Peng, and G. Cheng (2014), Stable carbon isotopes as indicators for permafrost carbon vulnerability in upper reach of Heihe River basin, northwestern China, *Quat. Int.*, *321*, 71–77, doi:10.1016/j.quaint.2013.12.001.
Mu, C., T. Zhang, Q. Wu, B. Cao, X. Zhang, X. Peng, X. Wan, L. Zheng, Q. Wang, and G. Cheng (2015), Carbon and nitrogen properties of permafrost over the Eboling Mountain in the upper reach of Heihe River Basin, northwestern China, *Arct. Antarct. Alp. Res.*, *47*(2), 203–211, doi:10.1657/AAAR00C-13-095.
Mu, C., T. Zhang, X. Zhang, B. Cao, X. Peng, L. Cao, and H. Su (2016a), Pedogenesis and physicochemical parameters influencing soil carbon and nitrogen of alpine meadows in permafrost regions in the northeastern Qinghai-Tibetan Plateau, *Catena*, *141*, 85–91, doi:10.1016/j.catena.2016.02.020.
Mu, C., T. Zhang, X. Zhang, L. Li, H. Guo, Q. Zhao, L. Cao, Q. Wu, and G. Cheng (2016b), Carbon loss and chemical changes from permafrost collapse in the northern Tibetan Plateau, *J. Geophys. Res. Biogeosci.*, *121*, 1781–1791, doi:10.1002/2015JG003235.
Munroe, J. S., J. A. Doolittle, M. Z. Kanevskiy, K. M. Hinkel, F. E. Nelson, B. M. Jones, Y. Shur, and J. M. Kimble (2007), Application of ground-penetrating radar imagery for three-dimensional visualisation of near-surface structures in ice-rich permafrost, Barrow, Alaska, *Permafrost Periglacial Processes*, *18*(4), 309–321, doi:10.1002/ppp.594.
Neal, A. (2004), Ground-penetrating radar and its use in sedimentology: Principles, problems and progress, *Earth Sci. Rev.*, *66*(3–4), 261–330, doi:10.1016/j.earscirev.2004.01.004.
Niu, F., Z. Lin, H. Liu, and J. Lu (2011), Characteristics of thermokarst lakes and their influence on permafrost in Qinghai-Tibet Plateau, *Geomorphology*, *132*(3–4), 222–233, doi:10.1016/j.geomorph.2011.05.011.
Outcalt, S. I., F. E. Nelson, and K. M. Hinkel (1990), The zero-curtain effect: Heat and mass transfer across an isothermal region in freezing soil, *Water Resour. Res.*, *26*(7), 1509–1516, doi:10.1029/WR026i007p01509.
Pang, Q., G. Cheng, S. Li, and W. Zhang (2009), Active layer thickness calculation over the Qinghai-Tibet Plateau, *Cold Reg. Sci. Technol.*, *57*(1), 23–28, doi:10.1016/j.coldregions.2009.01.005.
Parsekian, A. D., L. Slater, and D. Giménez (2012), Application of ground-penetrating radar to measure near-saturation soil water content in peat soils, *Water Resour. Res.*, *48*, W02533, doi:10.1029/2011WR011303.
Peng, X., T. Zhang, B. Cao, Q. Wang, K. Wang, W. Shao, and H. Guo (2016), Changes in freezing-thawing index and soil freeze depth over the Heihe River Basin, Western China, *Arct. Antarct. Alp. Res.*, *48*(1), 161–176, doi:10.1657/AAAR00C-13-127.
Schwamborn, G., D. Wagner, and H.-W. Hubberten (2008), The use of GPR to detect active layers in young periglacial terrain of Livingston Island, Maritime Antarctica, *Near Surf. Geophys.*, *6*(5), 331–336.
Shiklomanov, N., F. Nelson, D. Streletskiy, K. Hinkel, and J. Brown (2008), The Circumpolar Active Layer Monitoring (CALM) program: Data collection, management, and dissemination strategies, paper presented at 9th International Conference on Permafrost, edited by D. L. Kane and K. M. Hinkel.
Smith, M. W., and D. W. Riseborough (2002), Climate and the limits of permafrost: A zonal analysis, *Permafrost Periglacial Processes*, *13*(1), 1–15, doi:10.1002/ppp.410.
Stevens, C. W., B. J. Moorman, S. M. Solomon, and C. H. Hugenholtz (2009), Mapping subsurface conditions within the near-shore zone of an Arctic delta using ground penetrating radar, *Cold Reg. Sci. Technol.*, *56*(1), 30–38.
Tachikawa, T., M. Hato, M. Kaku, and A. Iwasaki (2011), Characteristics of ASTER GDEM version 2, paper presented at Geoscience and Remote Sensing Symposium (IGARSS) 2011 IEEE International, 24-29 July 2011.
Wang, Q., Z. Tingjun, J. Wu, X. Peng, X. Zhong, C. Mu, K. Wang, Q. Wu, and G. Cheng (2013), Investigation on permafrost distribution over the upper rechaes of Heihe River in the Qilian Mountains, *J. Glaciol. Geocryol.*, *35*(1), 19–29.
Wang, Q., T. Zhang, X. Peng, B. Cao, and Q. Wu (2015), Changes of soil thermal regimes in the Heihe River Basin over Western China, *Arct. Antarct. Alp. Res.*, *47*(2), 231–241, doi:10.1657/aaar00c-14-012.

Wang, Q., T. Zhang, H. Jin, B. Cao, X. Peng, K. Wang, L. Li, H. Guo, J. Liu, and L. Cao (2016), Observational study on the active layer freeze-thaw cycle in the upper reaches of the Heihe River of the north-eastern Qinghai-Tibet Plateau, *Quat. Int.*, doi:10.1016/j.quaint.2016.08.027, in press.

Wang, S., X. Chen, and Z. Zhang (1995), Permafrost distribution in the Dabanshan pass section of Ning-Zhang Highway in Eastern Qilian Mts. [J], *J. Glaciol. Geocryol.*, *17*(2), 184–188.

Westermann, S., U. Wollschläger, and J. Boike (2010), Monitoring of active layer dynamics at a permafrost site on Svalbard using multi-channel ground-penetrating radar, *Cryosphere*, *4*(4), 475–487, doi:10.5194/tc-4-475-2010.

Wieder, W., J. Boehnert, G. Bonan, and M. Langseth (2014), Regridded Harmonized World Soil Database v1. 2, edited.

Wollschläger, U., H. Gerhards, Q. Yu, and K. Roth (2010), Multi-channel ground-penetrating radar to explore spatial variations in thaw depth and moisture content in the active layer of a permafrost site, *Cryosphere*, *4*(3), 269–283.

Wu, J., Y. Sheng, H. Yu, and J. Li (2007), Permafrost in the middle east section of Qilian Mountains (I): Distribution of permafrost, *J. Glaciol. Geocryol.*, *29*(3), 418–425.

Wu, Q., and T. Zhang (2008), Recent permafrost warming on the Qinghai-Tibetan Plateau, *J. Geophys. Res.*, *113*, D13108, doi:10.1029/2007JD009539.

Wu, Q., and T. Zhang (2010), Changes in active layer thickness over the Qinghai-Tibetan Plateau from 1995 to 2007, *J. Geophys. Res.*, *115*, D09107, doi:10.1029/2009JD012974.

Wu, Q., T. Zhang, and Y. Liu (2012), Thermal state of the active layer and permafrost along the Qinghai-Xizang (Tibet) railway from 2006 to 2010, *Cryosphere*, *6*(3), 607–612.

Wu, T., S. Li, G. Cheng, and Z. Nan (2005), Using ground-penetrating radar to detect permafrost degradation in the northern limit of permafrost on the Tibetan Plateau, *Cold Reg. Sci. Technol.*, *41*(3), 211–219.

Wu, T., Q. Wang, M. Watanabe, J. Chen, and D. Battogtokh (2009), Mapping vertical profile of discontinuous permafrost with ground penetrating radar at Nalaikh depression, Mongolia, *Environ. Geol.*, *56*(8), 1577–1583, doi:10.1007/s00254-008-1255-7.

Wu, T., Q. Wang, L. Zhao, E. Du, W. Wang, O. Batkhishig, D. Battogtokh, and M. Watanabe (2012), Investigating internal structure of permafrost using conventional methods and ground-penetrating radar at Honhor basin, Mongolia, *Environ. Earth Sci.*, *67*(7), 1869–1876, doi:10.1007/s12665-012-1629-8.

Yoshikawa, K., C. Leuschen, A. Ikeda, K. Harada, P. Gogineni, P. Hoekstra, L. Hinzman, Y. Sawada, and N. Matsuoka (2006), Comparison of geophysical investigations for detection of massive ground ice (pingo ice), *J. Geophys. Res.*, *111*, E06S19, doi:10.1029/2005JE002573.

Zhang, T. (2005), Influence of the seasonal snow cover on the ground thermal regime: An overview, *Rev. Geophys.*, *43*, RG4002, doi:10.1029/2004RG000157.

Zhang, T., T. E. Osterkamp, and K. Stamnes (1997), Effects of climate on the active layer and permafrost on the North Slope of Alaska, U.S.A., *Permafrost Periglacial Processes*, *8*(1), 45–67, doi:10.1002/(SICI)1099-1530(199701)8:1<45::AID-PPP240>3.0.CO;2-K.

Zhang, T., O. W. Frauenfeld, M. C. Serreze, A. Etringer, C. Oelke, J. McCreight, R. G. Barry, D. Gilichinsky, D. Yang, and H. Ye (2005), Spatial and temporal variability in active layer thickness over the Russian Arctic drainage basin, *J. Geophys. Res.*, *110*, D16101, doi:10.1029/2004JD005642.

Zhang, W., W. Cheng, Z. Ren, Y. Gao, J. Chen, B. Li, and C. Zhou (2014), Simulation of permafrost distributions in the Qilian Mountains using a multi-criteria approach, *Cold Reg. Sci. Technol.*, *103*, 63–73, doi:10.1016/j.coldregions.2014.03.010.

Zhao, C., Z. Nan, and G. Cheng (2005), Methods for modelling of temporal and spatial distribution of air temperature at landscape scale in the southern Qilian Mountains, China, *Ecol. Modell.*, *189*(1–2), 209–220, doi:10.1016/j.ecolmodel.2005.03.016.

Zhao, L., Q. Wu, S. S. Marchenko, and N. Sharkhuu (2010), Thermal state of permafrost and active layer in Central Asia during the international polar year, *Permafrost Periglacial Processes*, *21*(2), 198–207, doi:10.1002/ppp.688.

Zhou, J., W. Kinzelbach, G. Cheng, W. Zhang, X. He, and B. Ye (2013), Monitoring and modeling the influence of snow pack and organic soil on a permafrost active layer, Qinghai-Tibetan Plateau of China, *Cold Reg. Sci. Technol.*, *90–91*, 38–52, doi:10.1016/j.coldregions.2013.03.003.